KUNS 1337
April 21, 1995

RGM Study of the Hyperon-Nucleon Interaction in the SU_6 Quark Model I.

— Analysis of NN and Σ^+p Systems —

Yoshikazu Fujiwara

Department of Physics, Kyoto University, Kyoto 606-01

Choki Nakamoto

Graduate School of Science and Technology, Niigata University, Niigata 950-21

Yasuyuki Suzuki

Department of Physics, Niigata University, Niigata 950-21

Abstract

A unified description of the hyperon-nucleon interaction consistent with the NN interaction is given in the RGM formulation of the SU_6 quark model, in which the full Fermi-Breit interaction with explicit flavor symmetry breaking is incorporated. The medium-range central and long-range tensor components of the hyperon-nucleon interaction are augmented by the effective meson-exchange potentials generated from the scalar-meson nonet and π and K mesons of the Nijmegen model-F. With two parameters determined from the deuteron binding energy and NN $^1S_0$ phase shift, all the low-energy cross sections of the hyperon-nucleon interaction currently available are reasonably reproduced. The analysis of NN and Σ^+p systems is presented.

§1. INTRODUCTION

Although quantumchromodynamics (QCD) is now believed to be the correct theory of the strong interaction, it is still impossible to derive properties of mesons and baryons and their interactions from this first principle. Many investigations of low-energy hadronic phenomena in nuclear physics, therefore, have been carried out by using QCD-inspired effective models such as the phenomenological quark model and the Skyrme model. In particular, the nucleon-nucleon (NN) interaction is one of the most important phenomena of the strong interaction, for which numerous efforts have already been devoted to overcome some difficulties of the meson-exchange description, such as the short-range repulsion and the phenomenological form factors of meson-baryon couplings. In the quark-model study of the NN interaction, the resonating-group method (RGM) is successfully employed to isolate short-range repulsion between two three-quark ($3q$) systems, originating from the color-magnetic contact (U^{GC}) term of the Fermi-Breit interaction and the effect of the Pauli principle related to the internal structure of the nucleons.[1] Owing to the explicit introduction of quark degrees of freedom, this framework is versatile enough to extend our vast knowledge of the NN interaction to the less-investigated hyperon-nucleon (YN) interaction by utilizing the fact that the hyperons and nucleons belong to a common class of the spin-flavor SU_6 supermultiplet 56.

The importance of the spin-flavor symmetry in the YN interaction is most extensively explored in our recent study on the central part of this interaction.[2] It is well known that the ($3q$)-($3q$) RGM in its naive form is not able to reproduce the important medium-range attraction responsible for the nuclear binding. The model is, therefore, inevitably supplemented with some phenomenological ingredients which are usually supposed to represent meson-exchange effects well established in the long-range region. The question raised in Ref. 2) is what kind of medium-range attraction is required in order to make possible a simultaneous description of the NN and YN interactions. This question can be answered only if we succeed in diminishing the ambiguities of quark-model potentials with the help of

rich spin-flavor symmetries carried by these interactions. In order to achieve this, we have introduced in Ref. 2) a couple of simplifications as in the following:

1) The spatial wave function of the $(3q)$ cluster is assumed to be a simple $(0s)^3$ wave function with a common harmonic-oscillator constant b, while the flavor symmetry breaking (FSB) of the quark-model Hamiltonian is explicitly incorporated with no approximation.

2) The quadratic-type confinement potential is employed to cut off the source of the extra FSB due to the phenomenological confinement mechanism.

3) The full Fermi-Breit interaction up to the order of $(v/c)^2$ is taken into account. This means that Galilean non-invariant terms like the momentum-dependent retardation term (U^{MC}) are also retained, since they are the consequence of the Lorentz invariance of the original relativistic interaction Lagrangian.

4) The effect of the channel coupling between ΛN and ΣN channels for the isospin $I = 1/2$ system is neglected, since it is found to be rather moderate if the non-central forces are not introduced.

5) The sum of the kinetic-energy and U^{MC} exchange kernels is renormalized with the ratio of the calculated and empirical reduced masses. This prescription has a couple of advantages, among which the most important one is that the correct kinematics is ensured with the use of the empirical mass. These modified exchange kernels give us quite stable results against the approximation of the quark Hamiltonian employed in the calculation.

As a result of these assumptions, we can follow up the change of the phase-shift behavior with respect to the continuous variation of the FSB parameter, $\lambda = (m_s/m_{ud})$. This is important, since some simple SU_3 relations for the interaction in various baryon configurations and channels are usually no longer valid if the FSB is introduced.

The result of the analysis in Ref. 2) implies that the flavor-independent attraction generated from the ϵ-meson exchange potential of the Nijmegen model-D, for example, always leads to too much attractive behavior of the ΣN and ΛN phase shifts when the NN S-wave phase shift is adjusted to the empirical values. For example, the ^1S phase shift in the $\Sigma N(I = 3/2)$ channel is more attractive than that of the NN channel, even in the case of no FSB with $\lambda = 1$. This is caused by the smaller empirical reduced mass of the ΣN channel than that of the NN channel, since these two configurations have the same SU_3 content (22) and yield exactly identical exchange kernels for $\lambda = 1$. The increase of the λ value from unity does not improve this situation, since the effect of the FSB in all the important exchange kernels of the kinetic-energy, U^{MC} and U^{GC} terms simply increases the attraction of the $\Sigma N(I = 3/2)$ channel. We are, therefore, obliged to introduce weaker central attraction to the ΣN and ΛN channels than that to the NN channel. A possible explanation of these phenomena is that these central attractions we supply by hand are not actually due to the exchange of some "real" mesons, but just a simple replacement of more complicated processes like the two-pion exchange, π-ρ exchange, Δ-N or Δ-Λ excitations, and so on.

The role of the scalar-meson exchange potentials is strongly affected by the way to deal with the short-range repulsion even in the one-boson exchange potentials (OBEP). For example, in the Nijmegen model-F the hard core radii are determined by assuming that they are the same within the same SU_3 representation. On the contrary, the hard core radii in the model-D are adjustable parameters determined for each channel. This difference results in rather drastic reduction of scalar-meson induced central attraction needed in the Nijmegen model-F, in decreasing order from the NN system to the ΛN and ΣN systems. The finding in Ref. 2) is that, if we employ the scalar-meson nonet exchanges of the model-F as the effective meson-exchange potentials, we only need two adjustable parameters to get the overall fit of all the sixteen central phase-shift curves predicted by the model-F with just one exception. This exception is $\Sigma N(I = 3/2)$ ^1P phase shift, where very strong attraction is predicted in both model-F and model-D of the Nijmegen potentials.

The purpose of this and the next papers is to extend the previous study of the NN and YN central interaction to the realistic situation where all the non-central forces are incorporated in the complete coupled-channel RGM formalism. The calculated results are compared with the most recent phase shift analysis of the NN interaction and the experimental data for the low-energy YN scattering. The origin of these non-central forces is the non-central pieces of the Fermi-Breit interaction and the tensor force of the effective meson-exchange potentials. We have already found that the symmetric (sLS) and antisymmetric (aLS) LS forces of the Fermi-Breit interaction yield almost correct order of magnitude of the LS and $LS^{(-)}$ forces comparable to the ones predicted by Nijmegen potentials.[3] These are examined in the form of the Wigner transform of the quark exchange kernels with respect to each spin-parity state of the NN and YN systems. Since such an estimate is reliable for predicting the effect of the non-central kernels in RGM calculations, we omit the LS forces originating from the meson-exchange sector (mainly from the vector-meson exchanges). On the other hand, the tensor force originating from the Fermi-Breit interaction is known to be too small to explain very strong empirical values in the OBEP's.[4] This is confirmed not only for the one-pion exchange tensor force in the NN interaction, but also for the K-meson exchange tensor force acting in the ΛN and ΣN exchange diagrams. The inclusion of the π- and K-meson exchange tensor force is thus necessary for the realistic description of the experimental data. We will carry this out in a similar way to the effective meson-exchange potentials for the scalar mesons. The meson species and types of the interaction introduced in this study are, therefore, the central force of the scalar-meson nonet and the tensor force of the π and K mesons in the Nijmegen model-F. The effective meson-exchange potentials of these mesons are constructed first by assuming that a fictitious flavor-singlet meson is exchanged between two quarks and then by introducing the SU_3 relations to the coupling constants at the baryon level. We call this model RGM-F. In this paper we will discuss the simple case which does not cause any channel coupling; namely, the NN system and the $\Sigma N(I = 3/2)$ system. The ΛN-$\Sigma N(I = 1/2)$ system with channel coupling involves an extra complication in the proper treatment of the coupling terms of the effective meson-exchange

potentials and the reduced mass problem, and will be discussed in the next paper.

The organization of this paper is as follows. In the next section we discuss some important features of the RGM-F, focussing on the RGM treatment of the effective meson-exchange potentials with respect to the central and tensor forces. An approximate treatment of the Coulomb force in the pp and Σ^+p systems is also briefly discussed. The phase-shift behavior of the NN system and some of the deuteron properties are discussed in Section 3.1. The RGM-F predictions for the $\Sigma N(I = 3/2)$ phase shifts are given in Section 3.2., together with the low-energy Σ^+p cross sections and the total nuclear scattering cross sections up to $p_{lab} = 1$ GeV/c. It is found that the total nuclear scattering cross sections show a big difference between our result and the prediction by the Nijmegen potentials in the intermediate-energy region of $p_{lab} = 400 \sim 600$ MeV/c. The effective range parameters of the pp, np and Σ^+p systems are also discussed in these subsections. The final section is devoted to a brief summary.

§2. FORMULATION OF THE EFFECTIVE MESON-EXCHANGE POTENTIALS IN RGM-F

Our RGM equation with the effective meson-exchange potentials is formulated by adding various pieces of the standard meson-exchange potentials $\mathcal{V}^{(\Omega)}$ acting between quarks to the qq interaction H_{qq} in Eq. (3.3) of Ref. 2); $H_{qq} \to H_{qq} + \Sigma_\Omega \mathcal{V}^{(\Omega)}$. For the scalar-meson central ($\Omega = CN$) and the pseudo-scalar-meson tensor ($\Omega = TN$) forces, these are given by

$$\mathcal{V}^{(CN)}(\boldsymbol{r}) = -g^2\, m\, Y(x) \ ,$$
$$\mathcal{V}^{(TN)}(\boldsymbol{r}) = f^2\, \frac{m}{3}\, S_{12} \left[Z(x) - \frac{4\pi}{m^3}\, \delta(\boldsymbol{r}) \right] \ , \qquad (2.1)$$

where $S_{12} = 3\,(\boldsymbol{\sigma}_1 \cdot \hat{\boldsymbol{r}})\,(\boldsymbol{\sigma}_2 \cdot \hat{\boldsymbol{r}}) - (\boldsymbol{\sigma}_1 \cdot \boldsymbol{\sigma}_2)$, m is the corresponding meson mass, and $Y(x) = e^{-x}/x$, $Z(x) = (1 + 3/x + 3/x^2)\, Y(x)$ with $x = m|\boldsymbol{r}|$. In Eq. (2.1), we have assumed that the exchanged mesons are flavor-singlet for the simplicity of the presentation, but the flavor-dependence is introduced later in g^2 and f^2 at the baryon level. If we neglect the flavor

dependence of the coupling constants, the calculation of the quark exchange kernel is quite straightforward and the resultant RGM equation is given by (see Eqs. (3.17) $\sim$ (3.19) of Ref. 2))

$$\left[\varepsilon_\alpha + \frac{\hbar^2}{2\mu_\alpha}\left(\frac{\partial}{\partial \boldsymbol{R}}\right)^2 - V_{\alpha D}^{(CN)}(\boldsymbol{R}) - V_{\alpha D}^{(TN)}(\boldsymbol{R})\, S_{12} \right] \chi_\alpha(\boldsymbol{R})$$
$$= \sum_{\alpha'} \int d\boldsymbol{R}' \left[\sum_{\Omega} \mathcal{M}^{(\Omega)}_{\alpha\alpha'}(\boldsymbol{R},\boldsymbol{R}') - \varepsilon_\alpha\, \mathcal{M}^{N}_{\alpha\alpha'}(\boldsymbol{R},\boldsymbol{R}') \right] \chi_{\alpha'}(\boldsymbol{R}') \ , \qquad (2.2)$$

where S_{12} is now the tensor operator with respect to $\boldsymbol{R}$ and the quark exchange kernel $\mathcal{M}^{(\Omega)}_{\alpha\alpha'}(\boldsymbol{R},\boldsymbol{R}')$ with $\Omega = K,\ MC,\ CC,\ GC,\ sLS,\ aLS$ and T should be further extended to include the meson-exchange contributions with $\Omega = CN$ and TN. We note that the effective meson-exchange potentials contain the direct terms $V_{\alpha D}^{(\Omega)}(\boldsymbol{R})$, since the $\mathcal{V}^{(\Omega)}$ terms of Eq. (2.1) do not contain the color factor $(\lambda_1^C \cdot \lambda_2^C)$ unlike the quark-model qq interaction. These direct potentials are given by

$$V_{\alpha D}^{(CN)}(\boldsymbol{R}) = -9\ g^2\ m\ Y_{\alpha_0}(x) \ ,$$
$$V_{\alpha D}^{(TN)}(\boldsymbol{R}) = f^2\ \frac{m}{3}\left[\, Z_{\alpha_0}(x) - D_{\alpha_0}(x)\right] \ , \qquad (2.3)$$

where $Y_{\alpha_0}(x)$, $Z_{\alpha_0}(x)$, etc. with $\alpha_0 = (mb)^2/3$ are the standard OBEP functions with the Gaussian form factor $F(q^2) = \exp\{-(bq)^2/6\}$. The expressions of these functions as well as the exchange kernels $\mathcal{M}^{(\Omega)}_{\alpha\alpha'}(\boldsymbol{R},\boldsymbol{R}')$ with $\Omega = CN$ and TN are given in Appendix. It should be noted that the internal-energy contribution from the central force, $E_{int}^{(CN)} = -9\ g^2\ m\ Y_{\alpha_E}(0)$ with $\alpha_E = (3/2)\alpha_0$, is carefully subtracted from the exchange kernel as usual, while the tensor term has no contribution since we have assumed $(0s)^3$ configuration for the $(3q)$ clusters. Furthermore, the exchange kernels $\mathcal{M}^{(K)}_{\alpha\alpha'}(\boldsymbol{R},\boldsymbol{R}')$ and $\mathcal{M}^{(MC)}_{\alpha\alpha'}(\boldsymbol{R},\boldsymbol{R}')$ in Eq. (2.2) should be modified into $\widetilde{\mathcal{M}}^{(K)}_{\alpha\alpha'}(\boldsymbol{R},\boldsymbol{R}')$ and $\widetilde{\mathcal{M}}^{(MC)}_{\alpha\alpha'}(\boldsymbol{R},\boldsymbol{R}')$ given in Eq. (4.2) of Ref. 2), in order to use the empirical reduced mass for μ_α. This is straightforward for the single-channel problems with $\alpha = \alpha'$ discussed in this paper.

The central issue in this section is how to introduce the flavor dependence in the effective meson-exchange potentials. From this and previous studies in Ref. 2), we have found that

the correct flavor dependence of the direct potentials is crucial to reproduce the empirical phase shifts predicted by successful OBEP's like the Nijmegen models. This is a natural consequence of the fact that the direct potential takes the form of the modified Yukawa functions, the interaction range of which is determined from the exchanged meson mass. On the contrary, the range of the exchange kernel is determined mainly by the harmonic-oscillator constant b, since each term of the exchange kernel is written as a product of the exchange normalization kernel and the modified Yukawa functions. (See Eq. (A4).) We, therefore, follow the procedure adopted in Ref. 2) and assume that the direct terms in Eq. (2.2) are proportional to the corresponding pieces of the Nijmegen model-F potential[5]. For the scalar-meson nonet employed in the model-F, this can be achieved by modifying $9\,g^2$ in Eqs. (2.3) and (A4) as

$$9\,g^2 \longrightarrow \begin{cases} c\ f_{a_3 a_1 \beta}\ f_{NN\beta} & \text{for} \quad \beta = \epsilon,\ S^* \quad \text{and} \quad \delta \ , \\ c\ f_{a_3 N\kappa}\ f_{a_1 N\kappa} \ , \end{cases} \qquad (2.4)$$

where a_3 and a_1 denote the hypercharge and the isospin to specify octet baryons in the bra and ket channels, respectively, (namely, $\alpha = [\frac{1}{2}(11)a_3, \frac{1}{2}(11)1\frac{1}{2}]SS_zYII_z;\mathcal{P}$ and $\alpha' = [\frac{1}{2}(11)a_1, \frac{1}{2}(11)1\frac{1}{2}]SS_zYII_z;\mathcal{P}$) and $f_{\alpha\alpha'\beta}$'s are Nijmegen model-F coupling constants determined from the SU_3 parameters of the scalar-meson nonet through the SU_3 relations. Since the model-F possesses rather strong flavor dependence due to the singlet-octet meson mixing, we only need to introduce a common reduction factor c for each of the flavor states $\mathcal{P} = +1$ and $\mathcal{P} = -1$. A similar procedure can be used to generate necessary falvor dependence of the tensor force from the pseudo-scalar mesons. The model RGM-F discussed in this paper employs only π and K mesons to cure the shortage of the tensor force arising from the quark sector, and is a minimum model incorporating only the tensor component of these meson-exchange potentials. After some processes of trial and error, we have found no particular necessity to introduce any reduction or enhancement factors for the tensor component. The modification of f^2 in Eq. (2.3) and Eq. (A4) is, therefore,

$$f^2 \longrightarrow \left(\frac{m}{m_{\pi^+}}\right)^2 \begin{cases} f_{a_3 a_1 \pi}\, f_{NN\pi} \ , \\ f_{a_3 NK}\, f_{a_1 NK} \ , \end{cases} \tag{2.5}$$

where the appearance of the mass factor $(m/m_{\pi^+})^2$ is simply because the Nijmegen coupling constants are defined through the charged pion mass as the standard mass.

The explicit value of c in Eq. (2.4) is, of course, quite sensitive to the way of treating the tensor component of the effective meson-exchange potentials. We use the same value $c = 0.56$ as in Ref. 2) for $\mathcal{P} = 1$, but have found that the value $c = 0.33$ for $\mathcal{P} = -1$ previously determined from the NN ^3S central phase shift is too small to reproduce the deuteron binding energy. The final values we employ in RGM-F are

$$c = \begin{cases} 0.4212 & \text{for} \quad \mathcal{P} = -1 \quad (^3E \text{ or } ^1O) \ , \\ 0.56 & \text{for} \quad \mathcal{P} = +1 \quad (^1E \text{ or } ^3O) \ . \end{cases} \tag{2.6}$$

For the quark-model parameters, the same values as before [2] are used; namely, $b = 0.6$ fm, $m_{ud} = 313$ MeV, $\lambda = (m_s/m_{ud}) = 1.25$ and $\alpha_S = 1.5187$ determined from the correct Δ-N mass splitting through the color-magnetic interaction.

In this paper, we also introduce the Coulomb force to calculate the effective-range parameters and low-energy cross sections of the pp and $\Sigma^+ p$ systems. This can be done in a similar way to the central force discussed above. The direct potential is explicitly given by

$$V_{aD}^{(CL)}(\boldsymbol{R}) = Z_{a_1} Z_{a_2} \frac{e^2}{R} \, \mathrm{erf}(\sqrt{\gamma}\, R) \ , \tag{2.7}$$

where Z_{a_i} (i=1 or 2) is the electric charge in unit of e (i.e., $Z_{a_i} = I_{iz} + Y_i/2$), $\gamma = (3/4b^2)$ and erf(x) is the error function. The corresponding exchange kernel is given in Appendix. Although the treatment employed here is, of course, just an approximation for the exchange kernel, we believe that this is a reasonable one, since the Coulomb force is long-ranged and the flavor dependence of this force is rather simple.

§3. RESULTS AND DISCUSSION

3.1. The NN System

In the NN system, the flavor exchange symmetry $\mathcal{P}$ is uniquely specified by the conserved isospin value I through $\mathcal{P} = (-1)^{1-I}$. The choice of $c = 0.4212$ in $\mathcal{P} = -1$ case reproduces the binding energy of the deuteron, 2.22 MeV, through the $^3S_1$-$^3D_1$ channel-coupling by the tensor force. The calculated phase shifts of the $^3S_1$ and $^3D_1$ channels and the mixing angle ϵ_1 are shown in Fig. 1, together with the empirical data obtained by the most recent phase shift analysis by Stoks et al.[6] We see that, once the deuteron binding energy is correctly fitted, the behavior of the $^3S_1$ phase shift is also nicely reproduced up to the maximum incident energy $T_{lab} = 300$ MeV considered in the present investigation. The low-energy ϵ_1 values are a little overestimated compared with the empirical values, which seems to be a common feature of the quark-model approach incorporating the short-range nonlocal tensor kernel from the tensor component of the Fermi-Breit interaction.[7),8)]

Another parameter $c = 0.56$ for $\mathcal{P} = +1$ is the same value as is adopted in our previous study on the central force of the NN and YN interactions.[2] As is already discussed in the paper, the extreme low-energy part of the $^1S_0$ phase-shift is not attractive enough, since the present model does not consider the small but important long-range spin-spin central force from the one-pion exchange potential. This feature is further enhanced, if we include the Coulomb force for the pp scattering. This can be seen in the effective range parameters given in Table I, where the calculated value, $a_s = -5.85$ fm, obtained with the present approximate treatment of the Coulomb force is compared with the experimental value $a_s^{exp} = -7.81$ fm. In the same table, the scattering length a_t and the effective range parameter r_t for the $^3S_1$ state of the np system are also given. The agreement between the calculation and the experiment in this case is fairly good. On the other hand, the energy dependence of the $^1S_0$ phase shift is a little too weak in the energy region $T_{lab} > 200$ MeV, which is certainly related to the nature of the central attraction of the effective meson-exchange potentials

adopted in the present framework.

The $^3D_2$ phase shift in Fig. 2 shows that the tensor force in the intermediate-range region seems to be too strong in this particular channel, since the calculated phase shift at 300 MeV, for example, is about 35 degrees and is almost 10 degrees larger than the empirical value. The main reason of this over-estimation is probably due to the lack of the cancellation mechanism of the very strong one-pion tensor force and the ρ-meson exchange tensor force with the opposite sign. This is also one of the common features observed in the quark-model approach.[7),8)] Nevertheless, the splitting of the three ^3P_J states with $J = 0$, 1 and 2 are nicely reproduced as is seen in Fig. 3. The standard analysis on the phase-shift decomposition to the central, LS and tensor pieces given in Table II shows that the strength of each force is well controlled as long as these channels are concerned.

Figure 4 shows the behavior of the $^3F_2$ phase shift, the mixing angle ϵ_2 for $^3P_2$ - $^3F_2$ coupling and the $^1P_1$ phase shift. Although the detailed agreement of the calculated result with the experiment is still out of reach, the general feature of these phase shifts is reasonably reproduced.

3.2. The Σ^+p System

The phase-shift behavior of the $\Sigma N(I = 3/2)$ system in RGM-F is shown in Figs. 5 $\sim$ 10, together with that of the Σ^+p system predicted by the Nijmegen model-D (open circles) and model-F (crosses) potentials. The Coulomb force is neglected in these figures, since it does not seriously impair the result except at the extremely low energies. Since the phase-shift analysis of the YN interaction is not available, we will use these Nijmegen phase shifts as a gauge to measure the adequacy of our calculated result. In order to understand the characteristic behavior of the phase shifts, it is important to note the SU_3 content of each channel, as is discussed in Ref. 2). For example, the flavor symmetric states with $\mathcal{P} = +1$ ($^1S_0$, ^3P_J etc.) belong to the SU_3 state with (22), together with the $I = 1$ states of the NN system. As a result, the phase-shift behavior in these states should be very similar to that

of the NN system, as long as the Hamiltonian is approximately SU_3 scalar. This is indeed the case as is seen in Fig. 5 for $^1S_0$, Fig. 7 for $^1D_2$, Fig. 8 for $^3P_0$ and $^3P_2$, Fig. 9 for $^3P_1$, and Fig. 10 for $^3F_2$ and ϵ_2. In more detail, the $^1S_0$ phase shift in Fig. 5 is less attractive than that of the NN system shown in Fig. 2. It is discussed in Ref. 2) that the central attraction of the effective meson-exchange potentials for this system is necessarily much weaker than that of the NN system, since both the reduced-mass effect and the FSB of the quark-model Hamiltonian reduce the repulsive effect in the $\Sigma N(I = 3/2)$ system. Such a comparison is not possible for $\mathcal{P} = -1$ ($^3S_1$, $^3D_1$, $^1P_1$ etc.) states, since the SU_3 content for these states is (30) and is not equal to (03) for the $I = 0$ states of the NN system. For example, the effect of the Pauli principle is entirely different between the $\mathcal{P} = -1$ states of the $\Sigma N(I = 3/2)$ system and the $I = 0$ states of the NN system. In fact, the $^3S_1$ phase shift in Fig. 5 is strongly repulsive, corresponding to the very large negative value $X_N = -7/9$ for the spin-flavor-color factor of the exchange normalization kernel. Furthermore, the $^3D_1$ phase shift and the mixing angle ϵ_1 in Fig. 6 have the opposite sign to those of the NN system in Fig. 1.

It is interesting to note that the difference in the phase-shift behavior of the model-F and model-D is sometimes much larger than that between the predictions by RGM-F and by one of the Nijmegen potentials. For instance, the $^3S_1$, $^3D_1$ and ϵ_1 curves in Figs. 5 and 6 are closer to the predictions of the model-F rather than to those of the model-D. A similar thing is also found in $^1D_2$ and $^3D_2$ phase shifts in Fig. 7, $^3P_1$ phase shift in Fig. 9 and less prominently in ϵ_2 in Fig. 10. The $^3P_0$ curve shown in Fig. 8 is very close to both model-F and model-D results. Only exception of this rule is the $^3P_2$ phase shift in Fig. 8, where our result is apparently much closer to the model-D. However, the other counterpart $^3F_2$ and ϵ_2 of this $^3P_2$ - $^3F_2$ channel-coupling reproduce the characteristic behavior commonly seen in the model-F and model-D. Thus we reach the same conclusion found in our previous study on the LS forces of the YN interaction; namely, our results generally reproduce the predictions by the Nijmegen models, but when the model-D and the model-F predict different results, our quark model supports the predictions of the model-F.[3)] This is quite likely because the hard-core radii of the model-F is determined by assuming that they are the same within the

same SU_3 representations.[5] This assumption is naturally supported in our analysis of the spin-flavor-color factors of the quark exchange kernel, where the spin-flavor SU_6 symmetry of the octet baryons plays an essential role.[2]

A prominent feature of our calculation is that the $^1P_1$ phase shift shown in Fig. 9 is quite different from either the model-F or model-D prediction. With this only exception, the other phase-shift curves reproduce more or less the essential features of the Nijmegen model-F potential. As is discussed in Ref. 12), the Nijmegen $^1P_1$ Σ^+p potential is very attractive in the short range region and has very strong dependence on the hard core radius. Since this channel belongs to the SU_3 representation (30) and has no connection to the other ΣN and ΛN channels, they have used a small core-radius in order to reproduce the systematic rise of the experimental angular distribution at p_Σ = 160 - 180 MeV/c shown in Fig. 12.

On the other hand, such a strongly attractive behavior of the $^1P_1$ phase shift is very difficult to reproduce in the quark model. The reason for this is as follows. Let us simultaneously consider the $^1P_1$ phase shift of the present $\Sigma N(I = 3/2)$ system and the $^3P_1$ phase shift in the $\Sigma N(I = 1/2)$ system, since they have very similar attraction mechanism as long as the central parts of the potentials are concerned. The spin-flavor-color factors of the exchange normalization kernel in these channels are $X_N = 1/3$ and $X_N = 5/27$, respectively. The simple analysis[2] on the effect of the Pauli principle by the Saito model shows that the effective local potentials of the exchange kinetic-energy kernel as well as the contributions from the momentum-dependent retardation term U^{MC} are indeed attractive in the medium-range region in these channels, and the present $\Sigma N(I = 3/2)$ $^1P_1$ channel is more attractive than the other one. In the short-distance region, however, these potentials turn into repulsion due to the composite nature of the $3q$ structure. As the result, the above difference of the attraction in these channels is rather moderate, compared with the big difference given by the vector-meson exchange potentials in the Nijmegen model-F. In fact, if we turn on the other central pieces of the quark-model potentials as well as the effective meson-exchange

potentials, the ^1P phase shift of the $\Sigma N(I = 3/2)$ channel becomes less attractive than the ^3P phase shift of the $\Sigma N(I = 1/2)$ channel.[2] The inclusion of the non-central force changes the behavior of the $\Sigma N(I = 1/2)$ $^3P_1$ phase shift drastically particularly because of the very important effect of the $LS^{(-)}$ force in this $I = 1/2$ channel, which is the main subject discussed in the next paper. The $LS^{(-)}$ force in the present $\Sigma N(I = 3/2)$ system is very weak, since the $^1P_1$ and $^3P_1$ states belong to the different SU_3 states with (30) and (22), respectively.[3] Here, we only mention that the strength of the central attraction from the effective meson-exchange potentials is already fixed by the values of c in Eq. (2.6) determined in the NN sector, and there is very little possibility of changing the present conclusion by the ambiguities of the effective meson-exchange potentials. We have examined the effect of the spin-spin part contained in the pseudo-scalar meson-exchange potentials, which seems to play a partial role to increase the attraction in the $^1P_1$ state relative to the $^3P_1$ state. A preliminary analysis of this contribution turns out to raise the phase shift at most up to 30 degrees, which is still half of the Nijmegen predictions.

The big difference of the $^1P_1$ phase shifts predicted by the RGM-F and the Nijmegen model-F naturally results in the big difference of the Σ^+p scattering cross sections predicted by these models at the intermediate energies. This is shown in Fig. 11, where the nuclear part of the Σ^+p total scattering cross sections obtained in the RGM-F (solid curve) is compared with the predictions by the Nijmegen model-F (dashed curve)[5]. In the cross section calculations, we have included the Coulomb force in the approximate way as is described in Section 2. The partial waves up to the total angular momentum $J = 7$ are included. In the figure, the experimental data from Ref. 11) for the "total" cross sections are also plotted just for rough estimation. Although both models reproduce the existing data fairly well, a large difference shows up in the intermediate-energy region. Namely, the Nijmegen model yields a prominent bump around $p_\Sigma = 400 \sim 600$ MeV/c, while the RGM-F result shows a very smooth decreasing curve. For the detailed comparison with the experimental values of the total scattering cross sections, we have to average the differential cross sections over the measured angular range, as is done in the experimental analysis[11].

It turns out that the effect of the Coulomb force is less than 10 % in this energy region. For example, at 500 MeV/c, the calculated cross section is 51 mb for the nuclear part only, while it increases to 54 mb when the full differential cross sections are averaged over the angles from $\cos\theta_{min} = 0.5$ to $\cos\theta_{max} = -0.5$.

In order to show that the present RGM-F result reproduces the existing experimental data[11] reasonably well, we show in Figs. 12 and 13 the calculated angular distribution of the Σ^+p scattering at $p_\Sigma = 170$ MeV and the low-energy total scattering cross sections determined in the above procedure, respectively. In this energy region, dominant partial waves are $^1S_0$ and $^3S_1$ waves. In particular, the phase-shift rise of the $^1S_0$ channel in Fig. 5 up to the values around 30 degrees is quite essential in order to reproduce the magnitude of the cross sections. However, the reduction of the very strong repulsion of the $^3S_1$ channel due to the tensor coupling with the $^3D_1$ channel is also important not to make the cross sections too large. Regarding this situation, we compare in Table I the effective range parameters of these two S states with predictions of the other calculations and of effective-range analyses of the experimental cross sections. We find that the present model gives reasonable values except for r_t. For this quantity, even the sign is ambiguous, since this value is very sensitive to the detailed behavior of the curvature of the $^3S_1$ phase shift in the low-energy region. The P-wave phase shifts are generally very small in this energy region. For example, the $^1P_1$ phase shift at $p_\Sigma = 170$ MeV/c given in Ref. 12) is several degrees, while ours is less than one degree. Because of this small difference, the error bars of two data points in the backward angles in Fig. 12 do not cover the calculated curve by the RGM-F. Quite obviously, more accurate experimental measurements are necessary in order to draw more definitive conclusion on the behavior of the $^1P_1$ phase shift.

§4. SUMMARY

In this investigation we have extended our previous quark-model study on the central potentials of the nucleon-nucleon (NN) and the hyperon-nucleon (YN) interactions[2] by in-

corporating the non-central forces originating from the full Fermi-Breit interaction and the effective meson-exchange potentials of the pseudo-scalar meson type. Since our purpose is to gain consistent and comprehensive understanding of these interactions, the phenomenological input is restricted to a minimum as much as possible, without pursuing too much detailed description of the NN system. Furthermore, the flavor symmetry breaking (FSB) of the quark-model Hamiltonian as well as the reduced mass of the resonating-group (RGM) equation is carefully treated in order to diminish the ambiguity of the quark-model potentials. The meson species and types of the interaction introduced in this study are, therefore, the central force of the scalar-meson nonet in the Nijmegen model-F potentials and the tensor force of the π and K mesons. The effective meson-exchange potentials of these mesons are constructed first by assuming that a fictitious flavor-singlet meson is exchanged between two quarks and then by introducing the SU_3 relations to the coupling constants at the baryon level in such a way that the RGM direct potential becomes exactly the same as the Gaussian folding of the Nijmegen model-F potential. Since the scalar-meson exchange potentials are more or less phenomenological in any kinds of models, two common overall factors, c, are introduced for the central potentials depending on the symmetric or antisymmetric configuration of the flavor exchange symmetry, $\mathcal{P}$, with respect to the interchange of two octet baryons. These are determined in the NN sector; namely, from the deuteron binding energy (for $\mathcal{P} = -1$) and the $^1S_0$ phase shift (for $\mathcal{P} = +1$), and no further adjustment of these parameters is made in the calculation of the YN interaction. We call this model RGM-F, since all the meson parameters are taken over from the Nijmegen model-F potential.

In this paper, we have applied this framework to the NN and $\Sigma N(I = 3/2)$ systems, where no channel coupling occurs between the different YN systems. The Coulomb force is also incorporated to calculate the low-energy effective range parameters of the pp and Σ^+p systems and the Σ^+p scattering cross sections, in a similar way to the scalar-meson type effective meson-exchange potentials. With the two parameters determined at the S-state NN system, the phase-shift behavior of the other partial waves is reasonably reproduced. In particular, the RGM-F reproduces the correct ^3P_J splitting of the NN system due to the

well balanced contributions of the central, LS and tensor forces as a result of appropriate hybridization of the quark-model potentials and the effective meson-exchange potentials put in by hand.

In the $\Sigma N(I = 3/2)$ system, the phase-shift behavior predicted by the RGM-F is generally very similar to that of the Nijmegen model-F potential. This is a desirable condition, since the Nijmegen models are one of the most successful one-boson exchange potentials (OBEP) which can describe the detailed phase-shift behavior of the NN system and the available low-energy scattering data of the YN systems. Only one exception to this resemblance between the RGM-F result and the Nijmegen-model prediction is the $^1P_1$ phase shift, for which the OBEP description generally yields very strong attraction due to the vector-meson exchange potentials, while the RGM-F yields rather moderate attraction due to the attractive nature of the Pauli principle in this particular system. Although the RGM-F describes the low-energy Σ^+p scattering cross sections almost equally well to the Nijmegen models, the cross-section behavior at higher energies around $p_\Sigma = 400 \sim 600$ MeV/c shows a big difference from the prediction of the model-F due to the different behavior of this $^1P_1$ phase shift. We have found that the big bump of the total scattering cross sections in the model-F disappears in the RGM-F. Experimental data of the Σ^+p scattering cross sections in this energy range are quite useful to determine the correct behavior of the $^1P_1$ phase shift.

In the next paper, we will extend the RGM-F to the ΛN - $\Sigma N(I = 1/2)$ coupled-channel system, and examine the phase-shift behavior as well as the ΛN and Σ^-p scattering and reaction cross sections.

ACKNOWLEDGMENTS

The authors would like to thank members of Nuclear Theory Groups of Kyoto and Niigata Universities for useful discussions. They also would like to acknowledge the generous grants of computer time by the Research Center for Nuclear Physics, Osaka University. This work was supported by Grant-in-Aid for Scientific Research (C) from the Ministry of Education, Science and Culture (04640296).

APPENDIX: RGM EXCHANGE KERNEL OF THE EFFECTIVE MESON-EXCHANGE POTENTIALS

In this appendix, we show the explicit expressions of the RGM exchange kernel with respect to the meson-exchange qq interaction in Eq. (2.1) and the Coulomb force in some approximation. For the detailed derivation of these results, the recent exposition of the multicluster RGM formulation of Ref. 13) should be referred to. Here we only mention that these calculations are easily carried out by using the integral representation of the Yukawa function

$$\frac{\mathrm{e}^{-mr}}{r} = \frac{2}{\sqrt{\pi}} \int_0^\infty d\chi \, \exp\left\{ -\frac{m^2}{4\chi^2} - \chi^2 r^2 \right\} \quad , \tag{A1}$$

which is just an extension of the technique usually employed for the Coulomb kernels ($m = 0$ case). The modified Yukawa functions with the Gaussian form factor is nothing but a small modification of Eq. (A1). Namely, these functions appearing in the direct terms in Eq. (2.3) are given by

$$\begin{aligned}
Y_\alpha(x) &= \frac{1}{\sqrt{\pi}} \int_0^\infty du \left(\frac{1}{1+\alpha u^2} \right)^{\frac{3}{2}} \exp\left\{ -\frac{1}{u^2} - \frac{u^2}{1+\alpha u^2} \frac{x^2}{4} \right\} \\
&= \frac{\mathrm{e}^\alpha}{2x} \left[\mathrm{e}^{-x} \, \mathrm{erfc}\left(\sqrt{\alpha} - \frac{x}{2\sqrt{\alpha}} \right) - \mathrm{e}^{x} \, \mathrm{erfc}\left(\sqrt{\alpha} + \frac{x}{2\sqrt{\alpha}} \right) \right] \quad , \\
Z_\alpha(x) &= Y_\alpha(x) - \frac{3}{x} \frac{\partial}{\partial x} Y_\alpha(x) \\
&= \frac{1}{\sqrt{\pi}} \int_0^\infty du \left(\frac{1}{1+\alpha u^2} \right)^{\frac{3}{2}} \left[1 + \frac{3u^2}{2(1+\alpha u^2)} \right] \exp\left\{ -\frac{1}{u^2} - \frac{u^2}{1+\alpha u^2} \frac{x^2}{4} \right\} \\
&= \frac{\mathrm{e}^\alpha}{2x} \left[\left(1 + \frac{3}{x} + \frac{3}{x^2} \right) \mathrm{e}^{-x} \, \mathrm{erfc}\left(\sqrt{\alpha} - \frac{x}{2\sqrt{\alpha}} \right) - \left(1 - \frac{3}{x} + \frac{3}{x^2} \right) \mathrm{e}^{x} \, \mathrm{erfc}\left(\sqrt{\alpha} + \frac{x}{2\sqrt{\alpha}} \right) \right] \\
&\quad - \frac{3}{\sqrt{\alpha\pi}} \frac{1}{x^2} \exp\left\{ -\frac{x^2}{4\alpha} \right\} \quad , \\
D_\alpha(x) &= \frac{1}{2\sqrt{\pi}} \left(\frac{1}{\alpha} \right)^{\frac{3}{2}} \exp\left\{ -\frac{x^2}{4\alpha} \right\} \quad ,
\end{aligned} \tag{A2}$$

where $\mathrm{erfc}(x)$ is the complementary error function defined through

$$\mathrm{erfc}(x) = 1 - \mathrm{erf}(x) = \frac{2}{\sqrt{\pi}} \int_x^\infty \mathrm{e}^{-t^2} dt = \mathrm{e}^{-x^2} \left(\frac{1}{2x} - \frac{3}{4x^3} + \cdots \right) \quad , \tag{A3}$$

In Eq. (A2), $D_\alpha(x)$ corresponds to the δ-function part of the pseudo-scalar mesons.

The exchange kernels of the meson-exchange potentials in Eq. (2.1) are most easily expressed by using the operator formalism for the spin-flavor-color factors, $X^\Omega_{1\mathcal{T}}$, in the flavor space at the baryon level.[14),15)] When the internal-energy contribution is properly subtracted in the prior form as is shown in Eq. (3.19) of Ref. 2), these are given by

$$\mathcal{M}^{CN}(\boldsymbol{R}, \boldsymbol{R}') = -g^2 \, m \, \mathcal{M}^N(\boldsymbol{R}, \boldsymbol{R}') \left[-X^{CN}_{1S'} \, Y_{\alpha_E}(0) + \sum_{\mathcal{T} \neq E} X^{CN}_{1\mathcal{T}} \, Y_{\alpha_\mathcal{T}}(V_\mathcal{T}) \right] \quad ,$$

$$\mathcal{M}^{TN}(\boldsymbol{R}, \boldsymbol{R}') = f^2 \, \frac{m}{3} \, \widehat{\mathcal{M}}^N(\boldsymbol{R}, \boldsymbol{R}') \sum_{\mathcal{T} \neq E} X^{TN}_{1\mathcal{T}} \, [\, Z_{\alpha_\mathcal{T}}(V_\mathcal{T}) - D_{\alpha_\mathcal{T}}(V_\mathcal{T}) \,] \, S_{12}(\widehat{\boldsymbol{V}}_\mathcal{T}) \quad . \tag{A4}$$

Here, $\mathcal{T}$ denotes the five possible quark exchange diagrams, $\mathcal{T} = E$, S, S', D_+ and D_-, and the values $\alpha_\mathcal{T}$ and $\boldsymbol{V}_\mathcal{T}$ are given in Table III. In the tensor term, $S_{12}(\widehat{\boldsymbol{V}}_\mathcal{T})$ is the tensor operator with respect to $\widehat{\boldsymbol{V}}_\mathcal{T}$; i.e., $S_{12}(\boldsymbol{a}) = (\boldsymbol{\sigma}_1 \cdot \boldsymbol{a})(\boldsymbol{\sigma}_2 \cdot \boldsymbol{a}) - \boldsymbol{a}^2 (\boldsymbol{\sigma}_1 \cdot \boldsymbol{\sigma}_2)$. Furthermore, $\widehat{\mathcal{M}}^N(\boldsymbol{R}, \boldsymbol{R}')$ denotes the spatial part of the exchange normalization kernel; i.e., $\mathcal{M}^N(\boldsymbol{R}, \boldsymbol{R}') = X_N \, \widehat{\mathcal{M}}^N(\boldsymbol{R}, \boldsymbol{R}')$. The spin-flavor-color factors, $X^\Omega_{1\mathcal{T}}$, for the flavor-singlet mesons in Eq. (2.1) are very simple. For the central terms of the scalar meson, these are given by

$$X^{CN}_{1S} = X^{CN}_{1S'} = X^{CN}_{1D_+} = 4 \quad , \qquad X^{CN}_{1D_-} = 1 \quad , \tag{A5}$$

while for tensor terms of the pseudo-scalar meson these are

$$\begin{aligned} X^{TN}_{1S} &= X^{TN}_{1S'} = \frac{1}{6} \left[e^\dagger_m e_m - \frac{1}{2} \left(e^\dagger_e e_m + e^\dagger_m e_e \right) \right] \quad , \\ X^{TN}_{1D_+} &= -\frac{1}{12} \left(e^\dagger_e - e^\dagger_m \right) (e_e - e_m) \quad , \\ X^{TN}_{1D_-} &= -\frac{1}{6} \, e^\dagger_m e_m \quad , \end{aligned} \tag{A6}$$

where e_e and e_m are the electric- and magnetic-type SU_6 unit vectors defined in Eq. (A.16) of Ref. 15). The explicit values of the spin-flavor-color factors are easily calculated by using the product form of the SU_3 relations given in Eqs. (A.10) and (A.11) of Ref. 14), as well as some simple values of the SU_3-standard matrix elements of e_e and e_m given in Table I of the

same paper. Incidentally, the operator form of the spin-flavor-color factors for the exchange normalization kernel is given by $X_N = (-1/12) \, [\, e^\dagger_e e_e + (\boldsymbol{\sigma}_1 \cdot \boldsymbol{\sigma}_2) \, e^\dagger_m e_m \,]$.

The exchange kernel for the Coulomb force, $\mathcal{V}^{(CL)}(\boldsymbol{r}) = e^2 \, Q_1 \, Q_2 \, (1/r)$ with $Q_i = I_{iz} + Y_i/2$ $(i = 1, \, 2)$, is given by

$$\begin{aligned} \mathcal{M}^{CL}(\boldsymbol{R}, \boldsymbol{R}') = \widehat{\mathcal{M}}^N(\boldsymbol{R}, \boldsymbol{R}') \sqrt{\frac{2}{\pi}} \, \frac{e^2}{b} \, \Bigg\{ & X^{CL}_{1S'} \left[-1 + \sqrt{\frac{8}{5}} \, h_0 \left(\frac{3\gamma}{20} (3\boldsymbol{R}' - \boldsymbol{R})^2 \right) \right] \\ & + X^{CL}_{1S} \sqrt{\frac{8}{5}} \, h_0 \left(\frac{3\gamma}{20} (3\boldsymbol{R} - \boldsymbol{R}')^2 \right) + X^{CL}_{1D_+} \sqrt{2} \, h_0 \left(\frac{3\gamma}{4} (\boldsymbol{R} + \boldsymbol{R}')^2 \right) \\ & + X^{CL}_{1D_-} \sqrt{\frac{\pi}{6\gamma}} \, \frac{1}{|\boldsymbol{R} - \boldsymbol{R}'|} \Bigg\} \quad , \end{aligned} \tag{A7}$$

where $\gamma = (3/4b^2)$ and

$$h_0(a) = \int_0^1 \mathrm{e}^{-at^2} dt = \frac{\sqrt{\pi}}{2} \frac{1}{\sqrt{a}} \, \mathrm{erf}(\sqrt{a}) \quad . \tag{A8}$$

The exact evaluation of $X^{CL}_{1\mathcal{T}}$ is rather involved. However, if we use the same spirit of approximation as is used in the effective meson-exchange potentials, these are easily obtained as

$$X^{CL}_{1S} = X^{CL}_{1S'} = X^{CL}_{1D_+} = \frac{4}{9} \, Z_1 Z_2 \, X_N \quad , \qquad X^{CL}_{1D_-} = \frac{1}{9} \, Z_1 Z_2 \, X_N \quad , \tag{A9}$$

where Z_1 and Z_2 are charges of the two baryons in unit of e.

REFERENCES

[1] M. Oka and K. Yazaki, in *Quarks and Nuclei*, ed. W. Weise (World Scientific, Singapore, 1984), p.489 ; K. Shimizu, Rep. Prog. Phys. **52** (1989), 1 ; C.W. Wong, Phys. Rep. **136** (1986), 1.

[2] C. Nakamoto, Y. Suzuki and Y. Fujiwara, submitted to Prog. Theor. Phys. (1995).

[3] C. Nakamoto, Y. Suzuki and Y. Fujiwara, Phys. Letters **B318** (1993), 587.

[4] Y. Fujiwara and K.T. Hecht, Nucl. Phys. **A456** (1986), 669.

[5] M.M. Nagels, T.A. Rijken and J.J. de Swart, Phys. Rev. **D20** (1979), 1633.

[6] V. G. J. Stoks, R. A. M. Klomp, M. C. M. Rentmeester and J. J. de Swart, Phys. Rev. **C48** (1993), 792.

[7] K. T. Hecht and Y. Fujiwara, Nucl. Phys. **A463** (1987), 255c.

[8] S. Takeuchi, K. Shimizu and K. Yazaki, Nucl. Phys. **A504** (1989), 777.

[9] Zong-ye Zhang, Amand Faessler, U. Straub and L. Ya. Glozman, Nucl. Phys. **A578** (1994), 573.

[10] M.M. Nagels, T.A. Rijken and J.J. de Swart, Phys. Rev. **D15** (1977), 2547.

[11] F. Eisele, H. Filthuth, W. Föhlisch, V. Hepp and G. Zech, Phys. Letters **37B** (1971), 204.

[12] M. M. Nagels, T. A. Rijken and J. J. de Swart, Ann. Phys. **79** (1973), 338.

[13] Y. Fujiwara and Y. C. Tang, "Multicluster Resonating-Group Method of s-Shell Cluster Systems", Memoirs of the Faculty of Science, Kyoto University, Series A of Physics, Astrophysics, Geophysics and Chemistry, Vol. XXXIX, No. 1, Article 5 (1994), 91.

[14] Y. Fujiwara, Prog. Theor. Phys. Suppl. No. 91 (1987), 160.

[15] Y. Fujiwara, Prog. Theor. Phys. **88** (1992), 933.

[16] A. Reuber, K. Holinde and J. Speth, Nucl. Phys. **A570** (1994), 543.

[17] O. Dumbrajs, R. Koch, H. Pilkuhn, G. C. Oades, H. Behrens, J. J. de Swart and P. Kroll, Nucl. Phys. **B216** (1983), 277.

TABLES

TABLE I. The S-wave effective range parameters for NN and Σ^+p systems derived from RGM-F and the other models; Nijmegen model-D [10], model-F [5], and Jülich models A and B [16]. The Jülich result is without Coulomb force in Σ^+p, and the exp't denotes effective range analyses.

NN	$p\,p$		$n\,p$	
	a_s(fm)	r_s(fm)	a_t(fm)	r_t(fm)
RGM-F	−5.85	2.11	5.35	1.69
model-D	−7.814	2.670	5.431	1.771
model-F	−7.827	2.710	5.459	1.806
exp't [17]	−7.8098 ± 0.0023	2.767 ± 0.010	5.424 ± 0.004	1.759 ± 0.005
Σ^+p	a_s(fm)	r_s(fm)	a_t(fm)	r_t(fm)
RGM-F	−2.26	2.70	0.79	0.59
model-D	−3.66	3.52	0.34	−7.31
model-F	−3.20	3.87	0.70	−2.11
model-A	−2.26	5.22	−0.76	0.78
model-B	−1.09	10.20	−0.90	−1.24
exp't [12]	−2.42 ± 0.30	3.41 ± 0.30	0.709 ± 0.001	−0.783 ± 0.003

TABLE II. The phase-shift decomposition into the central, LS and tensor components in RGM-F for ^3P_J (J=0, 1, 2) states of the NN system. The RGM-F phase shifts in degrees are compared with the empirical values from the $p\,p$ analysis by Stoks et al. [6]

	T_{lab} (MeV)	25	50	100	150	200	300
^3P_C	RGM-F	1.63	3.29	4.36	3.60	2.28	−0.21
	exp't	0.69	1.76	2.75	2.48	1.56	−0.95
^3P_T	RGM-F	−1.82	−3.68	−5.52	−6.09	−6.28	−6.54
	exp't	−2.39	−3.73	−4.84	−5.26	−5.46	−5.58
$^3P_{LS}$	RGM-F	0.83	2.43	6.34	9.73	12.51	17.25
	exp't	0.84	2.61	6.33	9.39	11.89	15.88

TABLE III. The factors $\alpha_{\mathcal{T}}$ and the arguments $V_{\mathcal{T}}$ of the modified Yukawa functions in Eq. (A4) with respect to the five possible quark exchange diagrams, $\mathcal{T} = E,\ S,\ S',\ D_+$ and D_-.

$\mathcal{T}$	$\alpha_{\mathcal{T}}$	$V_{\mathcal{T}}$
E	$\frac{3}{2}\,\alpha_0$	0
S	$\frac{15}{16}\,\alpha_0$	$\frac{3}{8}\,m\,(3\boldsymbol{R}-\boldsymbol{R}')$
S'	$\frac{15}{16}\,\alpha_0$	$\frac{3}{8}\,m\,(3\boldsymbol{R}'-\boldsymbol{R})$
D_+	$\frac{3}{4}\,\alpha_0$	$\frac{3}{4}\,m\,(\boldsymbol{R}+\boldsymbol{R}')$
D_-	0	$\frac{3}{2}\,m\,(\boldsymbol{R}-\boldsymbol{R}')$

Figure Captions

Fig. 1 : The NN phase shifts for $^3S_1$ and $^3D_1$ channels and the mixing parameter ϵ_1 as functions of the laboratory energy. Experimental data are from Ref. 6).

Fig. 2 : Same as Fig. 1, except that the NN phase shifts are for $^1S_0$, $^3D_2$ and $^1D_2$ channels.

Fig. 3 : Same as Fig. 1, except for ^3P_J channels with $J = 0$, 1 and 2.

Fig. 4 : Same as Fig. 1, except for $^3F_2$ and $^1P_1$ channels and the mixing parameter ϵ_2 between $^3P_2$ and $^3F_2$ channels.

Fig. 5 : The $\Sigma N(I = 3/2)$ phase shifts for $^1S_0$ and $^3S_1$ channels as functions of the incident momentum in the laboratory system. The open circles denote the prediction of Nijmegen model-D [10], while the crosses that of the model-F [5].

Fig. 6 : Same as Fig. 5, except that the phase shift is for $^3D_1$ channel and ϵ_1 is the mixing parameter between $^3S_1$ and $^3D_1$ channels.

Fig. 7 : Same as Fig. 5, except for $^1D_2$ and $^3D_2$ channels.

Fig. 8 : Same as Fig. 5, except for $^3P_0$ and $^3P_2$ channels.

Fig. 9 : Same as Fig. 5, except for $^1P_1$ and $^3P_1$ channels. The mixing parameter ρ_1 due to the $LS^{(-)}$ force is far less than a degree over the whole range of energies, and is not shown.

Fig. 10 : Same as Fig. 5, except that the phase shift is for $^3F_2$ channel and ϵ_2 is the mixing parameter between $^3P_2$ and $^3F_2$ channels.

Fig. 11 : The total nuclear cross sections for Σ^+p scattering as predicted by RGM-F (solid curve) and by Nijmegen model-F (dashed curve) [5]. Experimental data are from Ref. 11).

Fig. 12 : Caluclated Σ^+p differential cross sections compared with the experimental data of Ref. 11).

Fig. 13 : Caluclated Σ^+p "total" cross sections compared with the experimental values of Ref. 11).

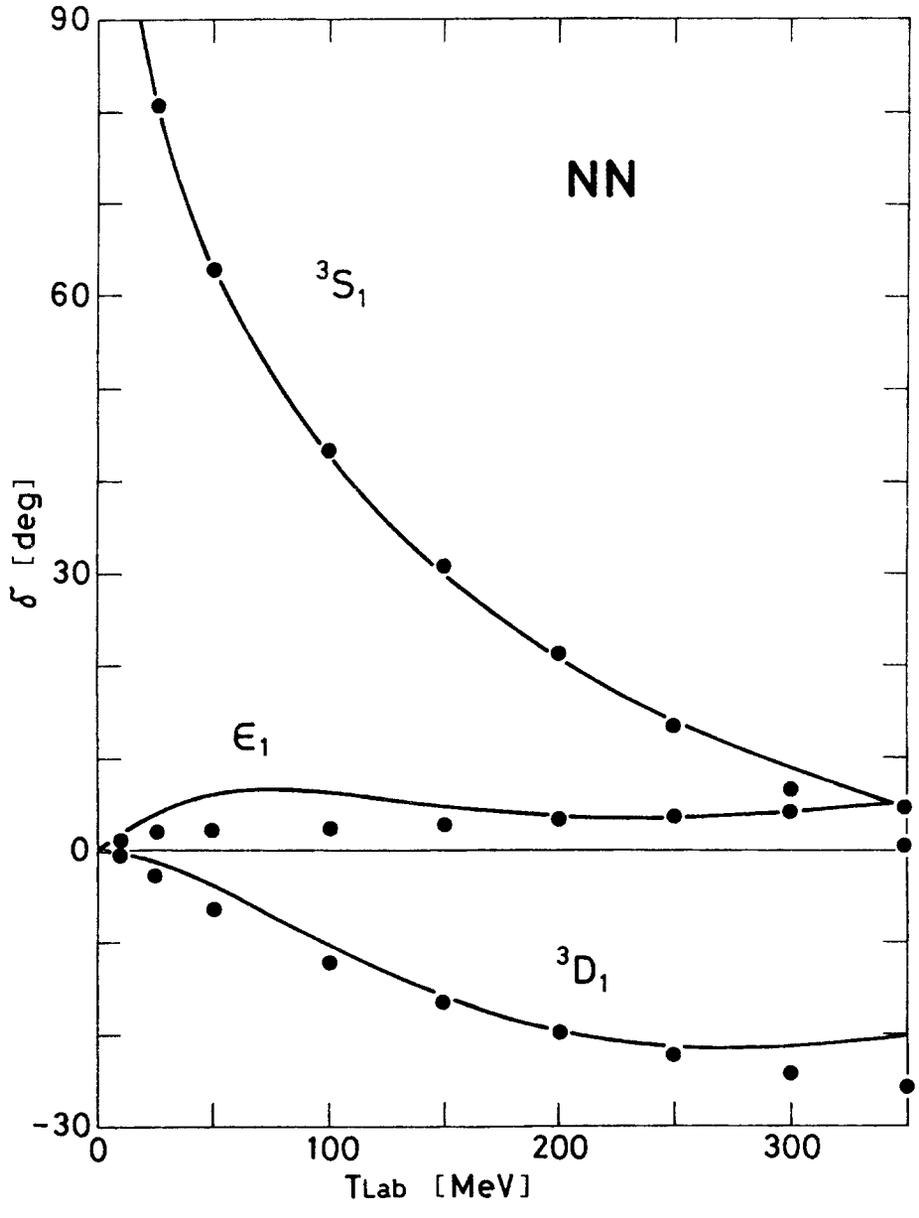
NN
$^3S_1$
ϵ_1
$^3D_1$
δ [deg]
90
60
30
0
-30
0
100
200
300
TLab [MeV]

Fig. 1

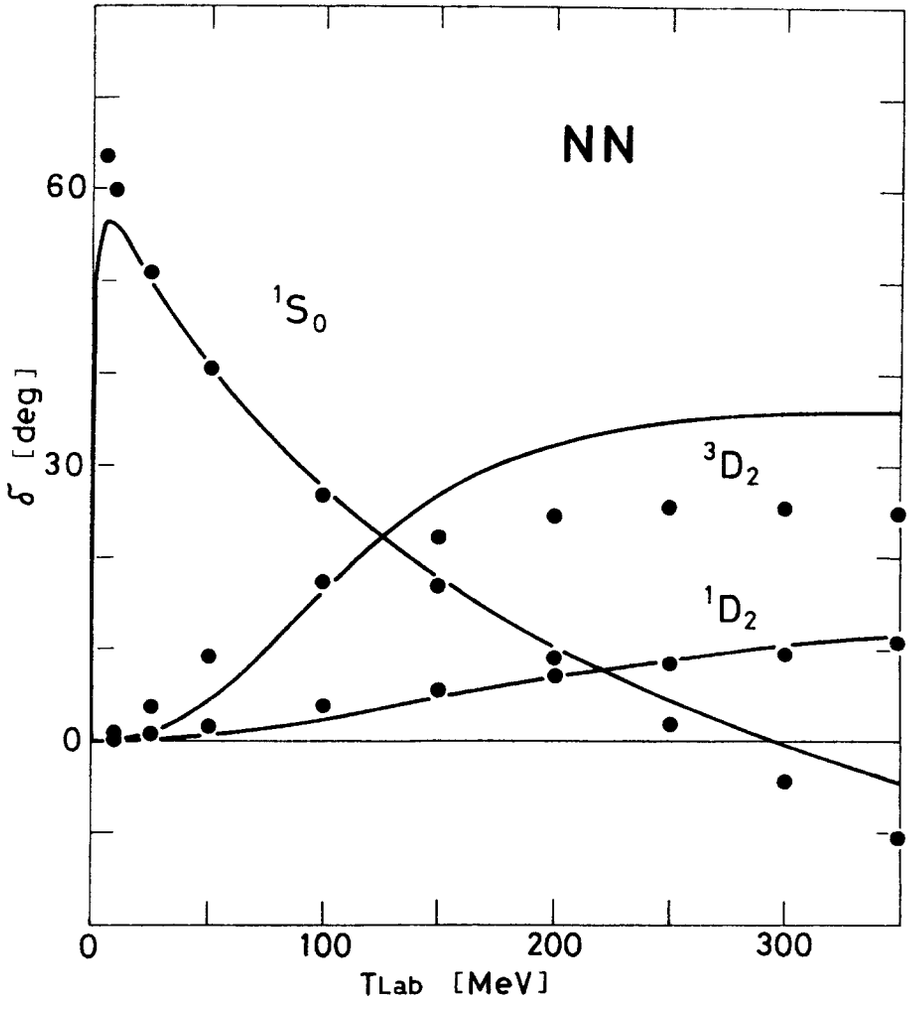
NN
$^1S_0$
$^3D_2$
$^1D_2$
δ [deg]
60
30
0
0
100
200
300
TLab [MeV]

Fig. 2

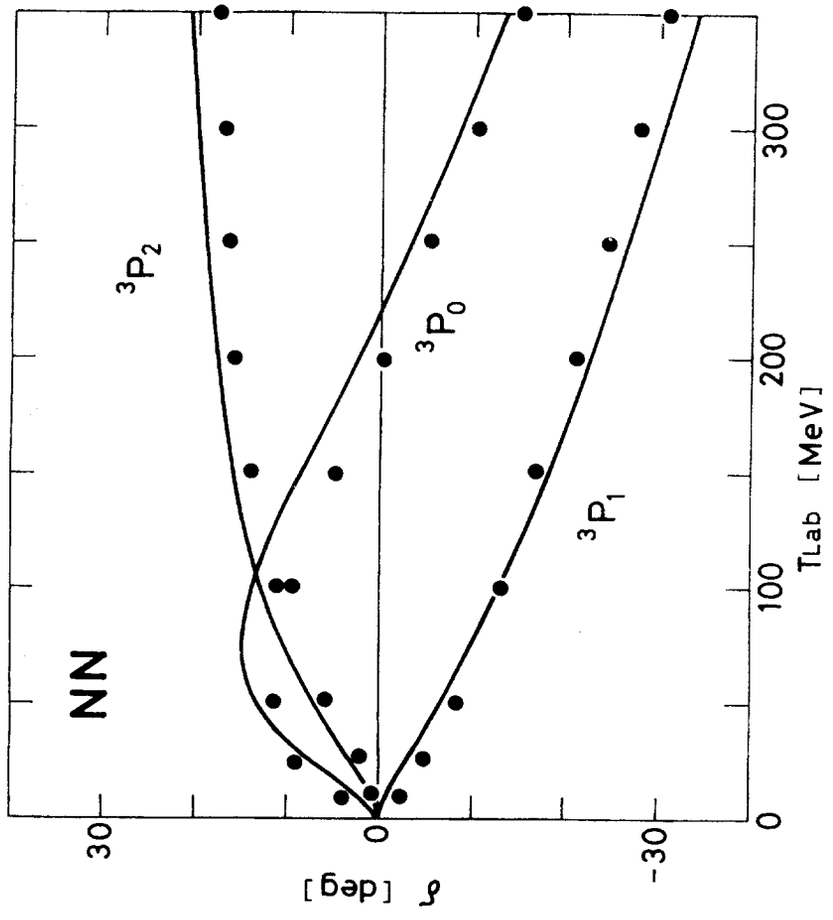
NN
$^3P_2$
$^3P_0$
$^3P_1$
δ [deg]
TLab [MeV]
30
0
-30
0
100
200
300

Fig. 3

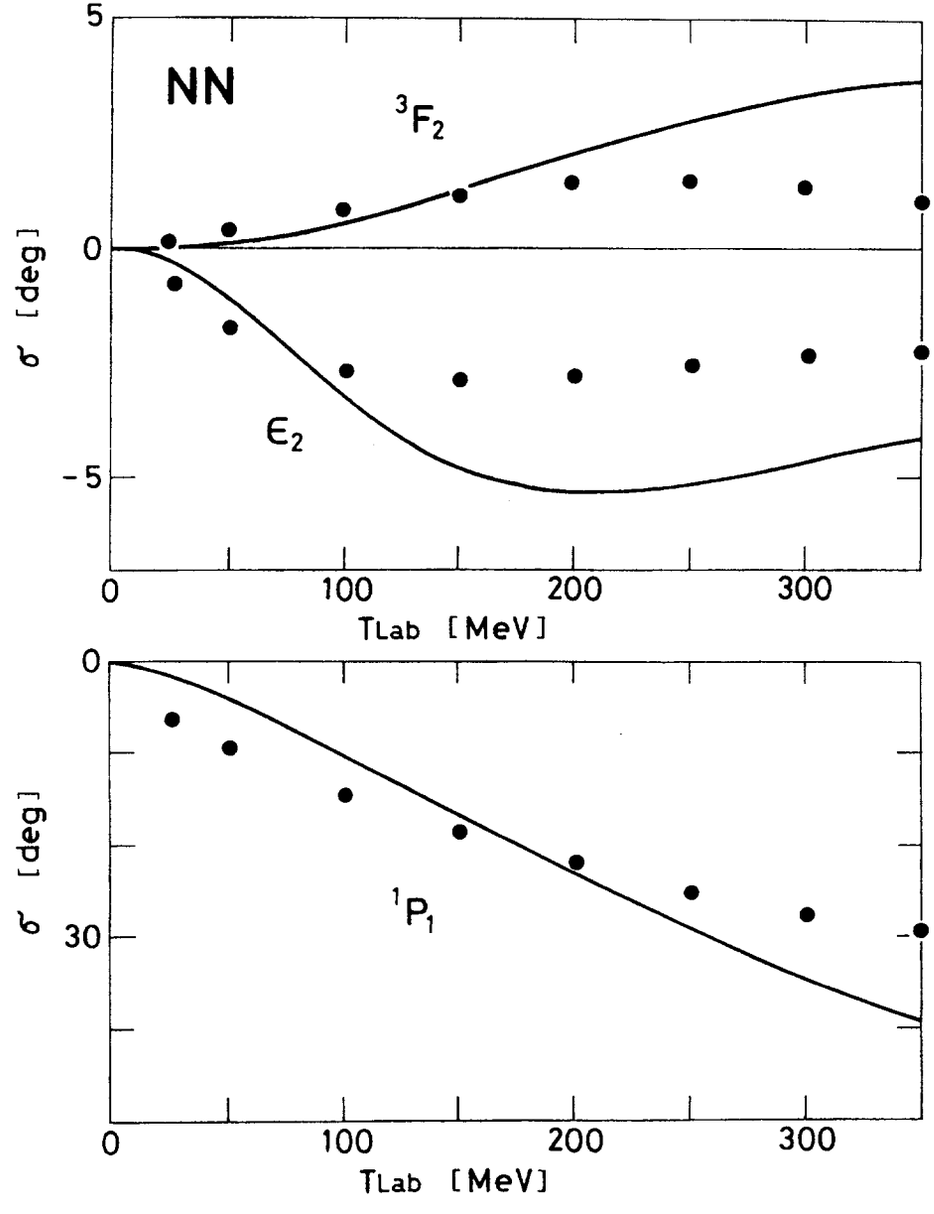
NN
$^3F_2$
ϵ_2
σ [deg]
TLab [MeV]
5
0
-5
0
100
200
300
$^1P_1$
σ [deg]
TLab [MeV]
0
30
0
100
200
300

Fig. 4

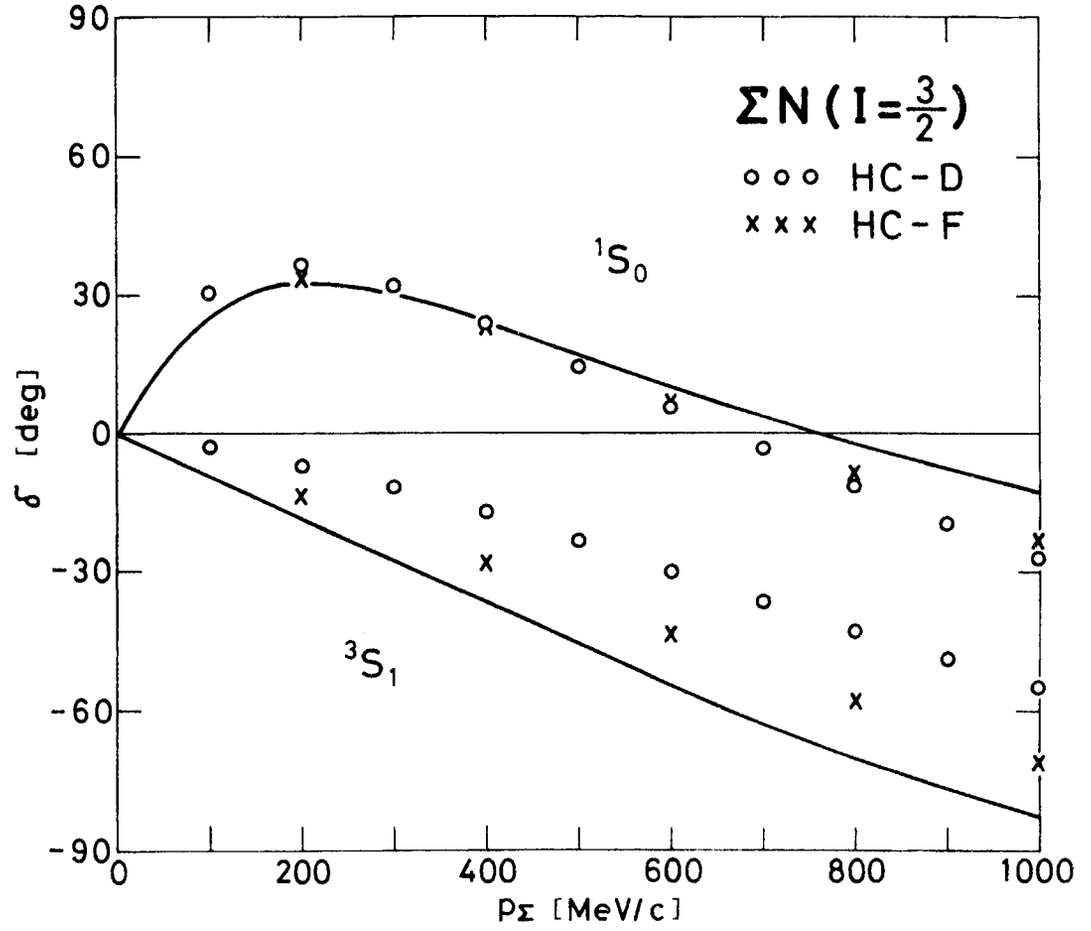
ΣN (I=3/2)
o o o HC-D
x x x HC-F
$^1S_0$
$^3S_1$
δ [deg]
Pσ [MeV/c]
90
60
30
0
-30
-60
-90
0
200
400
600
800
1000

Fig. 5

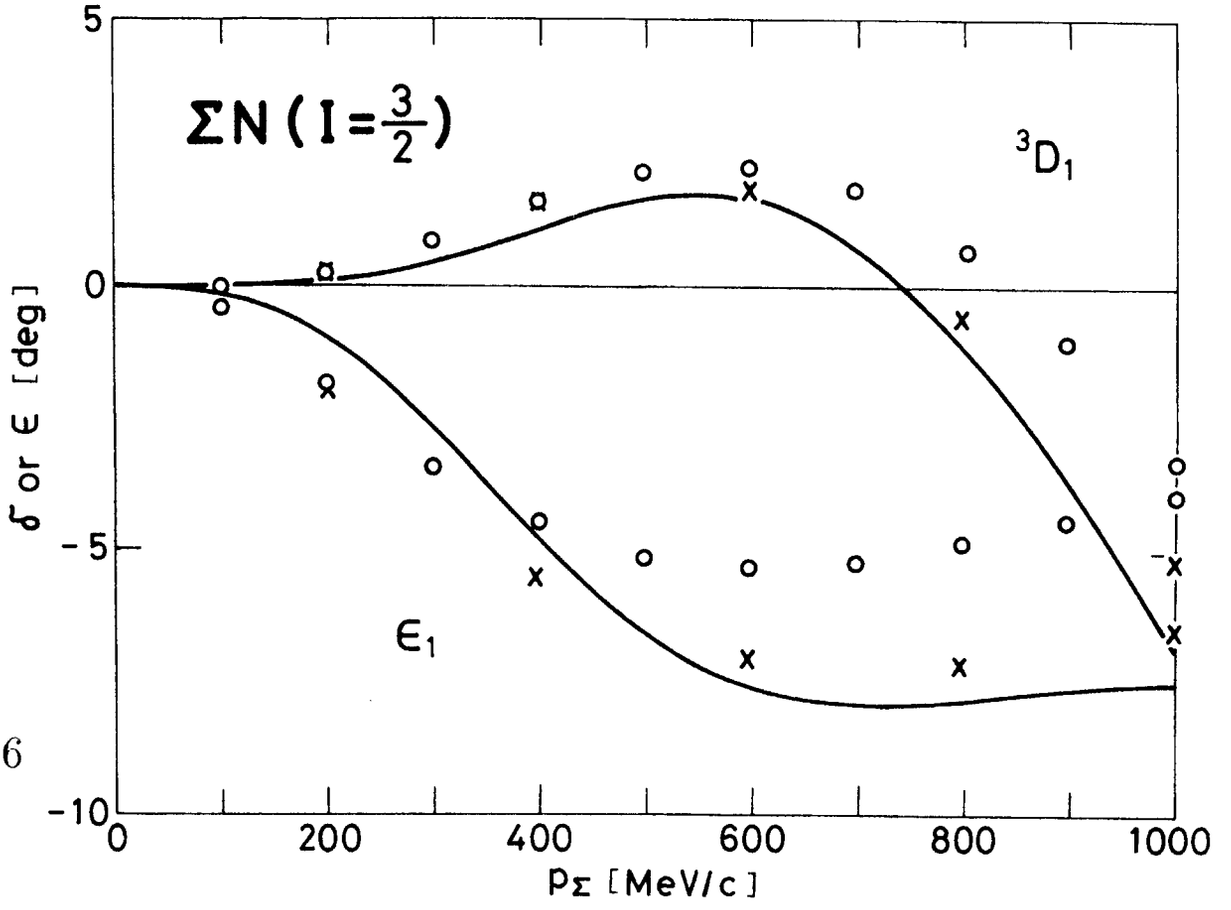
ΣN (I=3/2)
$^3D_1$
ϵ_1
δ or ε [deg]
Pσ [MeV/c]
5
0
-5
-10
0
200
400
600
800
1000

Fig. 6

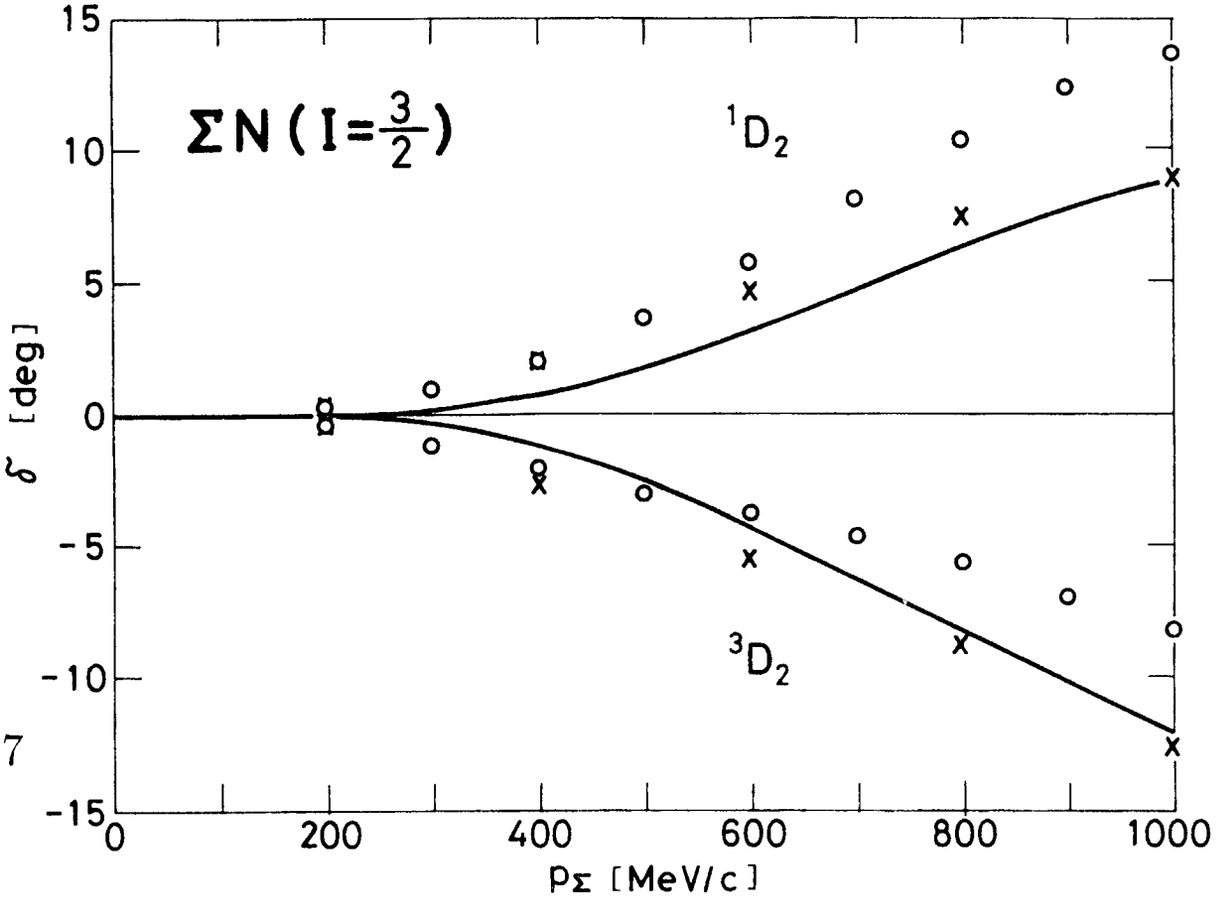
ΣN (I=3/2)
1D2
3D2
δ [deg]
PΣ [MeV/c]
15
10
5
0
-5
-10
-15
0
200
400
600
800
1000

Fig. 7

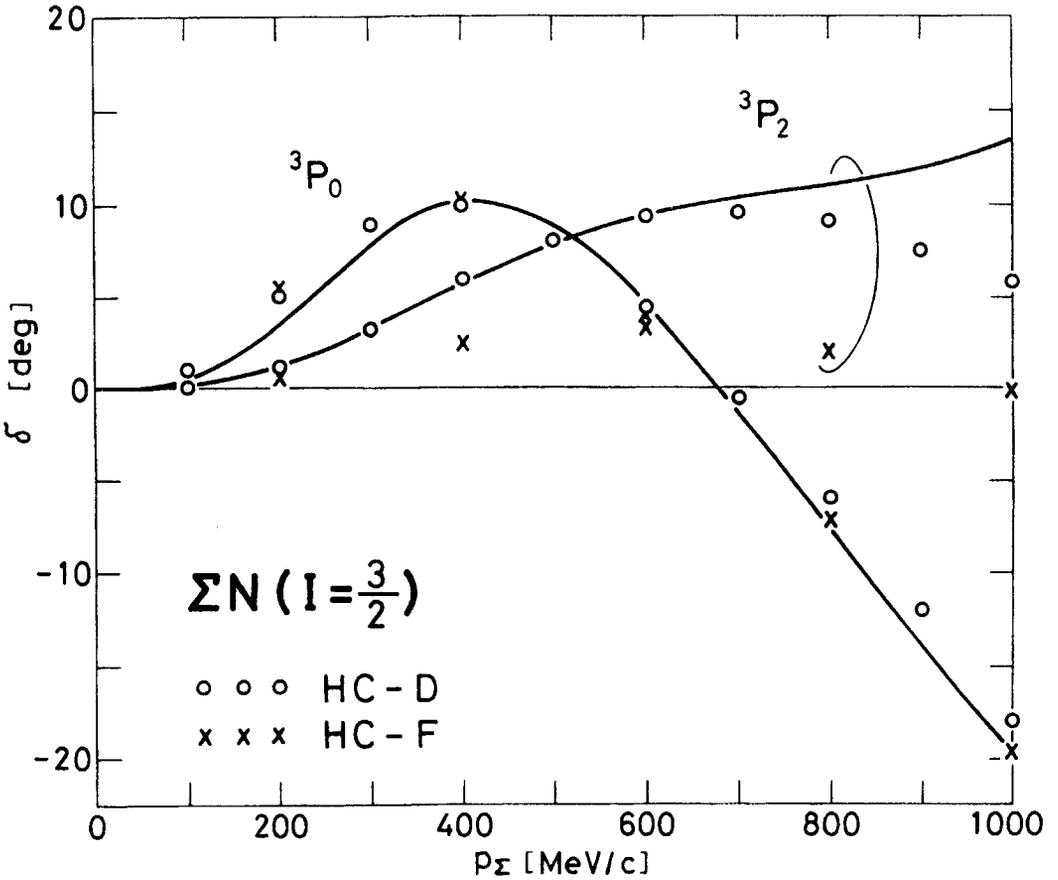
3P2
3P0
ΣN (I=3/2)
HC - D
HC - F
δ [deg]
PΣ [MeV/c]
20
10
0
-10
-20
0
200
400
600
800
1000

Fig. 8

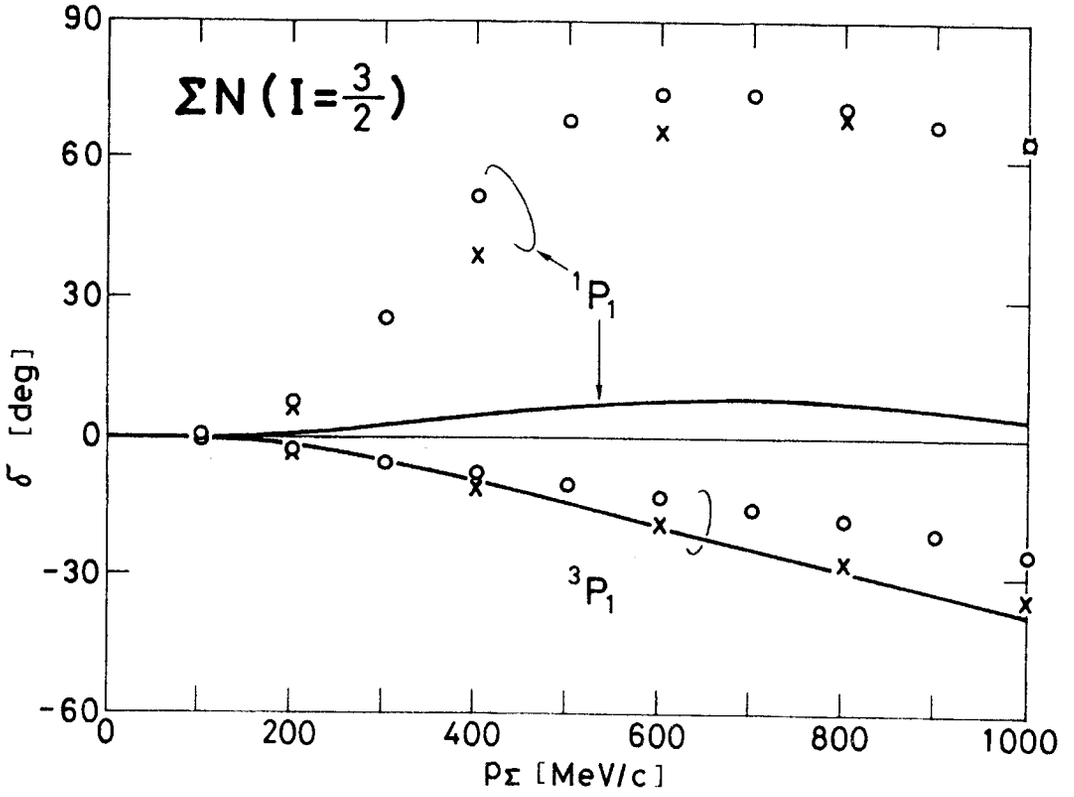
ΣN (I=3/2)
1P1
3P1
δ [deg]
Pσ [MeV/c]
90
60
30
0
-30
-60
0
200
400
600
800
1000

Fig. 9

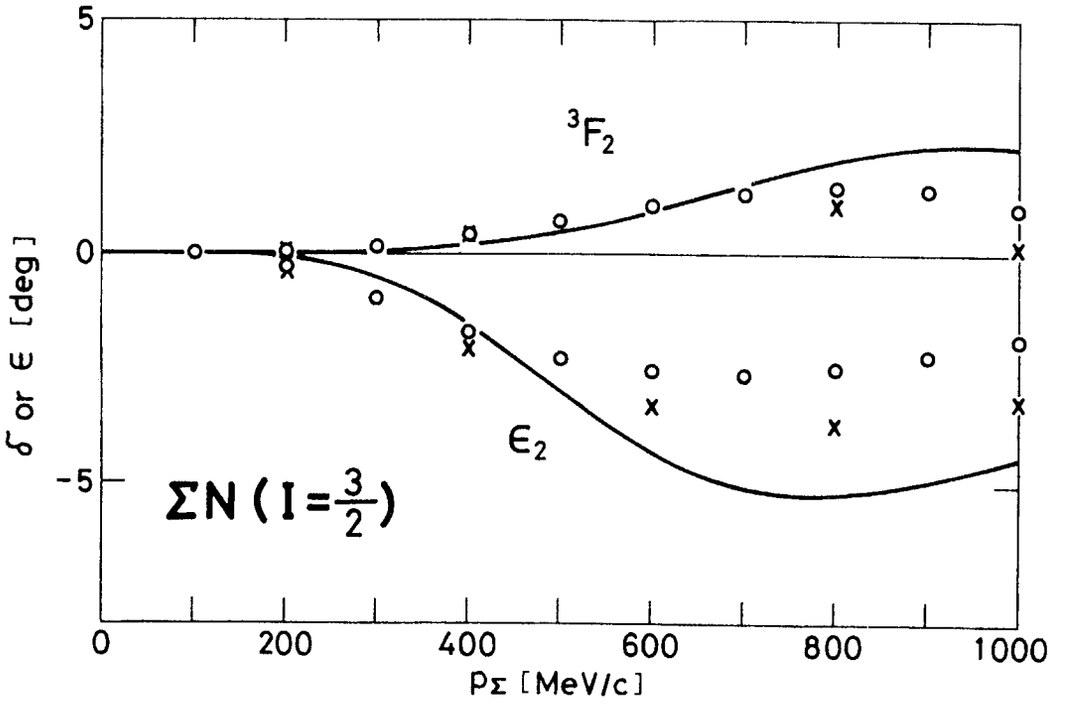
3F2
ε2
ΣN (I=3/2)
δ or ε [deg]
Pσ [MeV/c]
5
0
-5
0
200
400
600
800
1000

Fig. 10

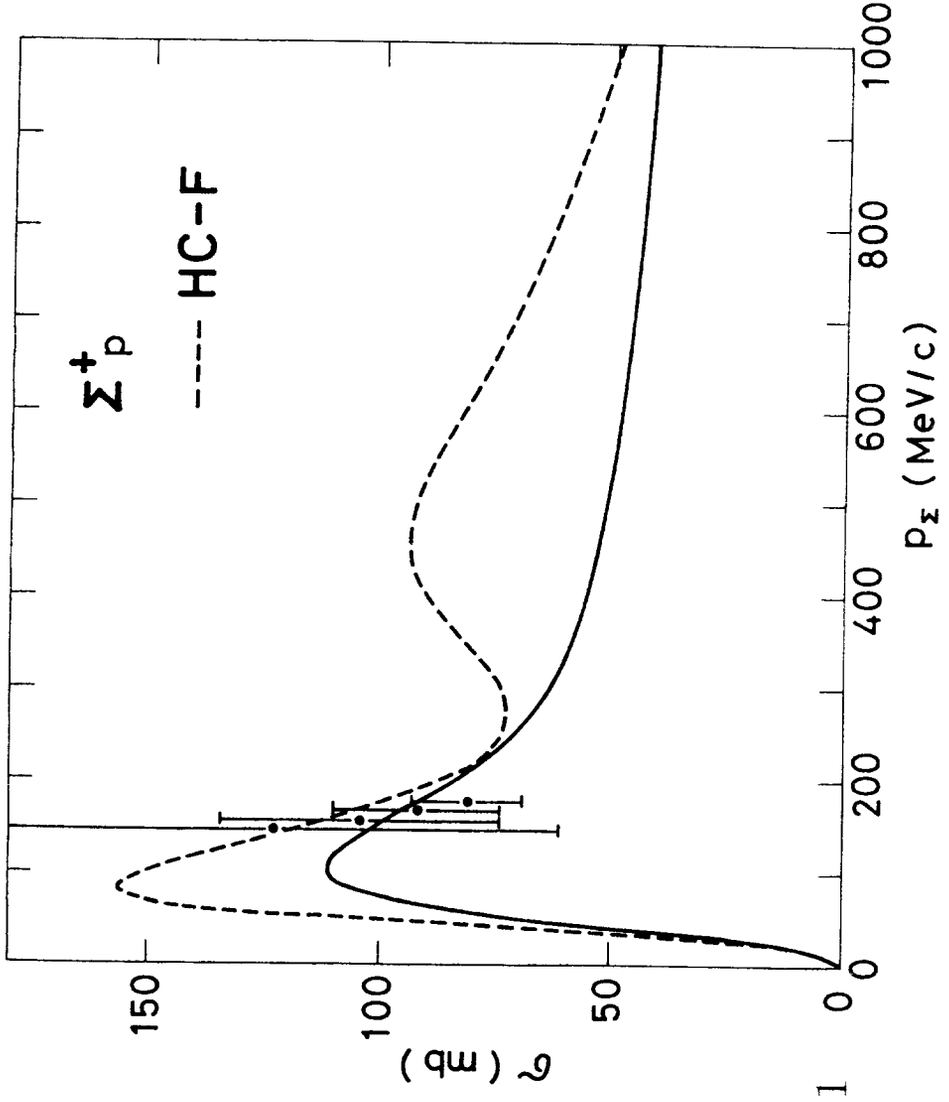
$\Sigma^+ p$
--- HC-F
σ (mb)
150
100
50
0
0
200
400
600
800
1000
p_Σ (MeV/c)

Fig. 11

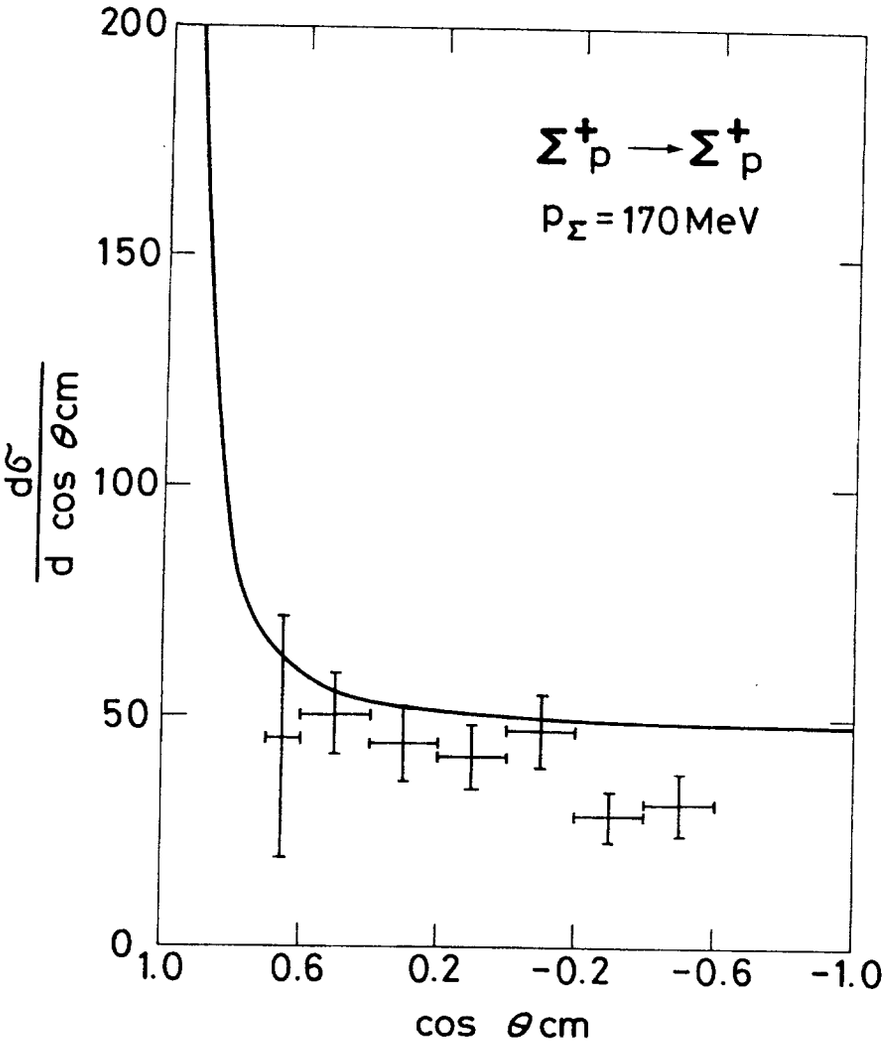
$\Sigma^+ p \rightarrow \Sigma^+ p$
$p_\Sigma = 170$ MeV
$\frac{d\sigma}{d \cos \theta cm}$
200
150
100
50
0
1.0
0.6
0.2
-0.2
-0.6
-1.0
cos θcm

Fig. 12

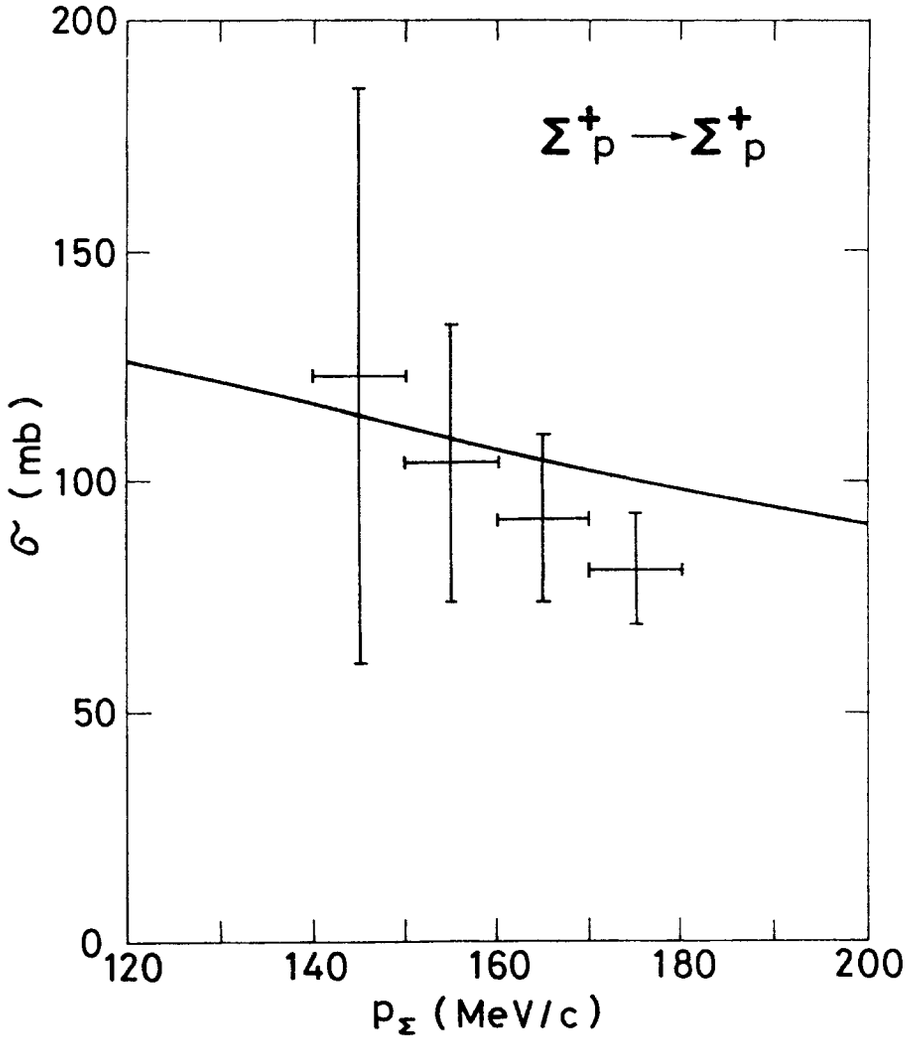

Fig. 13